

Pair-breaking effect caused by the anion disorder in the magnetic-field-induced spin-density wave: A calorimetric study

F. Tsobnang, F. Pesty, and P. Garoche

Laboratoire de Physique des Solides, Université de Paris-Sud, Bâtiment 510, 91405 Orsay cedex, France

(Received 10 May 1993; revised manuscript received 21 January 1994)

We have investigated the effect of anion disorder on the spin-density wave induced by the magnetic field (FISDW) in $(\text{TMTSF})_2\text{ClO}_4$ (the TMTSF is the tetramethyltetraselenafulvalene molecule). Specific heat and magnetocaloric-effect measurements have been performed under a magnetic field for various cooling rates across the ordering transition of the ClO_4 anions. The respective variations of the critical temperature and of the jump of the electronic specific heat at the metal-SDW transition are compared with the universal pair-breaking behavior of a Bardeen-Cooper-Schrieffer superconductor in the presence of *magnetic* impurities. The field-induced spin-density wave (FISDW), in the presence of *nonmagnetic* anion disorder, qualitatively behaves as the former but exhibits a stronger pair-breaking effect. The anion disorder is also shown to be responsible for the change in the criticality of the metal-SDW phase transition: a peculiar point in the phase diagram is found to evolve from tetracritical to bicritical as the anion disorder is increased. These behaviors are discussed in light of available models for the spin-density wave induced by the magnetic field.

I. INTRODUCTION

It is well known from Anderson's theorem that the thermodynamic properties of a conventional superconductor are nearly insensitive to nonmagnetic impurities.¹ On the contrary, the decrease in the electronic mean free path makes the mean-field approximation of the Bardeen-Cooper-Schrieffer (BCS) model² even more suitable.¹ On the other hand, magnetic impurities or an external magnetic field introduce perturbations that break the time-reversal symmetry, causing the destruction of Cooper pairs.³

This situation is different for a quasi-one-dimensional (Q1D) conductor, because of the nature of quasiparticle pairing. Pairs of particles, i.e., Cooper pairs for superconductivity, electron-hole pairs for charge-density waves (CDW) or spin-density waves (SDW), are supposed to form along individual molecular chains, but a three-dimensional ordered state can only be achieved at a finite temperature because of interchain coupling.⁴ It is well known that a system is more sensitive to thermodynamic or quantum fluctuations, or to defects as the space dimensionality is lowered. This statement holds for both superconductivity and spin-density waves in the case of a Q1D system.⁴ This is expected, and indeed observed in the molecular conductors: It has been reported that their low-temperature ground states are very sensitive to a very small amount of defects, induced either by x-ray irradiation or alloying.⁵

A more original situation arises from the anion disorder in the $(\text{TMTSF})_2\text{ClO}_4$ (where the TMTSF molecule is tetramethyltetraselenafulvalene). This compound exhibits at $T_{\text{AO}} = 24$ K a phase transition corresponding to the ordering of the noncentrosymmetric ClO_4 anions. The latter can exhibit two nonequivalent orientations, and the

structural modification corresponds to the doubling of the lattice period in the transverse direction b , with the wave vector $\mathbf{q} = (0, \frac{1}{2}, 0)$. This ordering transition displays kinetics effects: A very slow cooling across T_{AO} gives rise to a nearly complete ordering of the anions, whereas fast cooling leads to partly disordered domains,⁶ with a domain size directly proportional to the cooling rate.⁷ This kinetics yields strong effects on the low-temperature ground state. At zero magnetic field, for slow cooling rates, a superconducting state is stabilized below 1.2 K. But the latter is weakened for the faster cooling rates⁸ at the advantage of a spin-density wave (SDW) state.^{9,10}

The $(\text{TMTSF})_2\text{ClO}_4$ compound (at ambient pressure), as well as two other "Bechgaard salts," $(\text{TMTSF})_2\text{PF}_6$ and $(\text{TMTSF})_2\text{ReO}_4$ (above 10 kbars or around), exhibit at low temperature a cascade of magnetic phase transitions, as the magnetic field is varied from about 3–30 T or above.¹¹ According to the quantized-nesting model,¹¹ these transitions are believed to result from the quantization of the wave vector of a spin-density wave induced by the magnetic field (FISDW). The physical origin lies in the interference effect among three competing periodicities of the electronic system: the cyclotron, lattice, and SDW periods.¹¹ This quantization is associated with the observed 3D quantum Hall effect, and experimental evidences have been given that the quantum oscillations correspond to thermodynamic phases.¹¹

All the three salts behave differently as far as the anion ordering is concerned:¹² (1) No anion-ordering transition is observed in the PF_6 -based salt. This is related to the symmetry of inversion of the PF_6 group. (2) At ambient pressure, the ReO_4 -based salt undergoes a transition at $T_{\text{AO}} = 180$ K, characterized by a wave vector $\mathbf{q}_1 = (\frac{1}{2}, \frac{1}{2}, \frac{1}{2})$. The doubling of the lattice periodicity in the longitudinal direction gives rise to a metal-insulator

transition. The latter is suppressed above 12 kbars, as the ordering wave vector becomes $\mathbf{q}_2 = (0, \frac{1}{2}, \frac{1}{2})$, leading to the appearance of a superconducting state and a cascade of FISDW phases. No kinetics effect of the anion ordering has been reported in this salt.

(3) For the ClO_4 -based salt, the superconducting state is enhanced, and the FISDW phases are modified, as the anion order is improved by decreasing the cooling rate: For the slowest cooling rates, i.e., dT/dt below 2 K/h, negative plateaus of the Hall effect, the so-called “Ribault anomalies,”¹³ fine structure in the magnetization,¹⁴ tree-like phase diagram,^{15–17} as well as tetracritical behavior,^{18,19} have been reported. This means that the low-field FISDW phases are *avored* by anion ordering, like the superconducting state. However, the behavior of the FISDW is more subtle, because critical temperature is not the only physical quantity to be modified: New “fractional” phases appear as ordering is best achieved, and the very criticality of the metal-FISDW transition is involved.¹⁹

It must be pointed out that anion disorder may be considered as an *intrinsic* kind of disorder, similar to the composition disorder (obtained by alloying of different molecules or anions), and as opposed to *extrinsic* disorders, as irradiation-induced disorder, or defects, either due to chemical impurities or resulting from crystallographic imperfections during the synthesis process. Unlike the others, the anion disorder case provides us with an experimental “button,” due to the kinetics property of the transition in $(\text{TMTSF})_2\text{ClO}_4$, so that one is able to control the amount of “defects” by adjusting the cooling rate.

Precisely, this report aims at quantitatively studying the influence of this anion disorder on the phase transition between the normal metal and the FISDW in $(\text{TMTSF})_2\text{ClO}_4$. The specific heat is a powerful tool for such an investigation, thanks to the jump of the specific heat at such a second-order transition. Besides the changes in the critical temperature, the jump of the specific heat at the transition gives complementary information on the physical mechanism responsible for the transition. Moreover, investigations using measurements of the magnetocaloric effect allow us to describe the drastic sensitivity of the critical phenomena to the amount of anion disorder.

The structure of the article is the following. In Sec. II, a brief survey of used experimental techniques is given, concerning the cooling process, and the measurements of the heat capacity and of the magnetocaloric effect. In Sec. III, our experimental results are presented. First, the metal-FISDW transition is shown to be strongly affected by anion disorder. Second, experimental evidences of the tetracritical behavior are provided. Third, the complex influence of anion disorder on the phase diagram is detailed. Fourth, this behavior is coherently described in terms of the arising of a periodicity. Finally, the results are discussed in Sec. IV, within the framework of proposed theoretical models, and together with other experimental data. Emphasis is given on the sensitivity to disorder of the tetracritical behavior. The role of electronic mean free path is stressed.

II. EXPERIMENTAL TECHNIQUES

Calorimetric measurements have been carried out on a 2 mg single crystal of $(\text{TMTSF})_2\text{ClO}_4$, glued onto a 21-mg sample holder. The latter is made out from a sapphire slab, $0.3 \times 6 \times 2.5 \text{ mm}^3$, outfitted with a heater and a thermometer, deposited and designed by means of sputtering and microlithography techniques. The magnetic field was applied perpendicularly to an *a-b* face, i.e., along the crystallographic c^* direction.

A. Cooling the sample

The sample was cooled from 30 to 10 K using the following process: A linear voltage ramp was applied to the heater of the sample holder. This linear ramp yields a parabolic variation of the heating power as a function of the time: $P(t) \propto t^2$. The sample holder is linked to its thermal environment, at temperature $T_0 = 4.2 \text{ K}$, through a gold thin film (about 60 nm thick) deposited onto a mylar film ($1 \mu\text{m}$). At low temperature, the electronic mean free path is limited by the film thickness, and the thermal conductance K_b of this thermal link varies linearly with the temperature T : $K_b = 2\kappa T$, so that the heat losses integrated along the link vary as the square of temperature. As a result, the thermal balance during the cooling process becomes

$$C_{\text{tot}} \frac{dT}{dt} = P(t) - \kappa(T^2 - T_0^2), \quad (1)$$

where C_{tot} is the heat capacity of the assembly (sample plus sample holder), and dT/dt is the cooling rate, hereafter expressed in K/h. The coefficient κ was measured to be 53 nW/K^2 , using expression (1) at constant temperature ($dT/dt = 0$). The heating power was found to display a parabolic behavior as a function of a series of fixed temperatures, leading to a nearly temperature-independent κ in the 0.4–3 K range, within the experimental resolution (about 1%).

For cooling rates less than 10 K/h, the left member of the thermal balance (1) can be neglected, and the balance reads $P(t) \propto T^2 \propto t^2$. As a result, the cooling rate is approximately constant. This is well observed at the two slowest rates, 1.4 and 8 K/h, within 10%, less well for 90 K/h, within 20%, and badly for the fastest 300 K/h rate, within 50%. In the last two cases the cooling rate is determined at the $T_{\text{AO}} = 24 \text{ K}$ ordering temperature.

For each value of dT/dt , two kinds of calorimetric experiments were performed: specific-heat measurements as a function of the temperature, in fixed magnetic fields, and simultaneous measurements of the specific heat and the magnetocaloric effect as functions of a sweeping magnetic field, at a series of fixed temperatures.

B. Specific-heat measurements

The heat capacity C_p was measured in various fixed magnetic fields, from 4.5 to 5.5 T, as a function of the temperature, ranging from 0.4 to 1.3 K, using the con-

ventional ac technique.²⁰ The thermal frequency $f = \omega/2\pi$ was chosen to be 5 Hz, a convenient value for the internal thermal response time as well as the external response through the link. In the same range, the total heat capacity, sample plus sample holder, varies from 12 to about 130 nJ/K, and sample holder's heat capacity from 0.3 to 8 nJ/K (i.e., 3–6%). After subtracting the latter contribution, C_s (measured in a separate run), the low-temperature specific heat of the (TMTSF)₂ClO₄ sample in the metallic region, is found to be the sum of two terms: $C_s = C_{el} + C_{lat} = \gamma T + \beta T^3$. The linear term C_{el} is the conventional electronic contribution, and the cubic term C_{lat} arises from the lattice vibrations. The γ factor is directly proportional to the density of electronic states at the Fermi level, $N(E_F)$, and the β factor inversely proportional to the Debye temperature Θ_D cubed.²¹

The molar values are obtained using the mass of the sample, 2 mg, and the molar mass of (TMTSF)₂ClO₄, $M = 0.995$ kg. The coefficients are found to be $\gamma = 13 \pm 1$ mJ mol⁻¹ K⁻² and $\beta \approx 18$ mJ mol⁻¹ K⁻⁴. The coefficient γ is in good agreement with earlier measurements.^{22–24} Unlike the heater, the thin-film thermometer exhibits a (small) magnetoresistance (less than 6% between 0 and 7 T), that is corrected for all the presented measurements, using a calibration process of the thermometer in magnetic field. This calibration leads to small (a few %) residual oscillations, characterized by small curvatures of the metallic specific heat above 0.9 K, visible in Figs. 2 and 4. These oscillations are not physically meaningful, and only induce systematic errors (see the good experimental reproducibility and resolution, for instance in Fig. 2), and a small dispersion in the γ values (from 12.5 to 14 mJ mol⁻¹ K⁻² for the displayed fields).

Our present C versus T calorimetric experiments are consistent with previous measurements, that showed no significant variation of the β coefficient as a function of the magnetic field.^{23,24} The present dispersion in our C/T vs T^2 curves (a few percent, not shown) is not good enough to address the issue of the existence or not of a small variation. On the other hand, our C/T vs B experiments show unambiguously the absence of a variation of the α or β coefficients, within better than 1%. This is not displayed in the present article, but an example taken from the same run can be found in an independent article.¹⁹ In the latter, the specific heat C_{el}/T plotted versus the magnetic field B displays, below the threshold field, a metallic behavior characterized by a horizontal line of amplitude γ . The curves are found to be horizontal with a very good resolution.¹⁹ This means that in the normal-metal state, first, the contribution of the lattice vibrations to the specific heat is not observed to change as the magnetic field is varied, and second, that the density of electronic states $N(E_F)$ remains constant. However, we cannot rule out a possible (but not very probable) exact compensation of the two quantities.

The signal-to-noise ratio obtained for the magnetocaloric experiments is not as good as that of fixed field experiments, because the latter are performed using the superconducting magnet in its permanent mode, whereas the former require the use of a power supply to generate the varying current, so that an additional noise is present.

C. Magnetocaloric effect measurements

The ac calorimetry is well suited for the heat-capacity measurements as a function of an external parameter, e.g., a magnetic field.²⁰ Moreover, this technique can be adapted to simultaneously measure the heat exchanges produced by sweeping the field. This magnetocaloric effect is associated with the changes in entropy of a magnetic system. The heat absorbed or released by the sample is converted into a signal that can be measured by the thermometer, thanks to the low value of the thermal conductance K_b . This conductance limits the flow of the released power: $\Delta P = \Delta Q / \Delta t = K_b \Delta T$, and produces algebraic changes ΔT of the mean temperature \bar{T} of the sample. Knowing the value of the thermal conductance $K_b = 2\kappa T$ of the thermal link, the corresponding heat exchanges ΔQ can be determined to compute the entropy variations ΔS . In the case of reversible phase transformation, it becomes $\Delta S = \Delta Q / T$. The reversibility can be checked by comparing the data obtained for field swept up and down. Finally, the derivative versus the field, $\Delta S / \Delta B$, can be obtained. This is nothing else than the isofield coefficient of the magnetic moment, $\alpha_m = (\partial m / \partial T)_B = (\partial S / \partial B)_T$, thanks to the Maxwell-Weiss relation.²⁵ As a result, the coefficient α_m is directly proportional to the measured change in temperature ΔT :

$$\begin{aligned} \alpha_m &= \frac{\partial m}{\partial T} = \frac{\Delta S}{\Delta B} = \frac{\Delta Q / T}{v_B \Delta t} = \frac{\Delta P}{T v_B} = \frac{K_b \Delta T}{T v_B} \\ &= \frac{2\kappa}{v_B} \Delta T \propto \Delta T, \end{aligned} \quad (2)$$

where $v_B = dB/dt$ is the sweeping rate of the applied magnetic field B ; typically, $v_B = 3$ mT/s. The isofield coefficient for the magnetization, α_M , can then be deduced from α_m by using molar units (like the previous case of heat capacity). Multiply the magnetization α_m , expressed in J mol⁻¹ K⁻¹ T⁻¹, by 1000 to obtain α_M , expressed in emu mol⁻¹ K⁻¹ (i.e., ergs mol⁻¹ K⁻¹ G⁻¹). For example, to the largest $\partial M / \partial T$ anomaly in Fig. 5, of about 20 mJ mol⁻¹ K⁻¹ T⁻¹, corresponds a $\partial m / \partial T$ of about 40 nJ K⁻¹ T⁻¹. Relation (2) yields a corresponding temperature variation $\Delta T \approx 1$ mK. The variations are thus approximately isothermal, considering the average temperature of the experiment, 400 mK. Due to the small amplitude of ΔT , the contribution of the heat capacity to the heat exchanges has been checked to be less than 1% of the measured quantities, so that relation (2) leads to the determination of the magnetocaloric coefficient α_m with a good approximation.

The apparatus developed to measure C_p and α_M in the same experimental run will be described elsewhere.²⁶

III. EXPERIMENTAL RESULTS

A. Anion disorder and metal-FISDW transition

After subtracting the lattice contribution, the electronic specific heat is displayed in the Figs. 1 to 4 for a series of fixed magnetic fields, respectively, 4.5, 4.75, 4.90, and

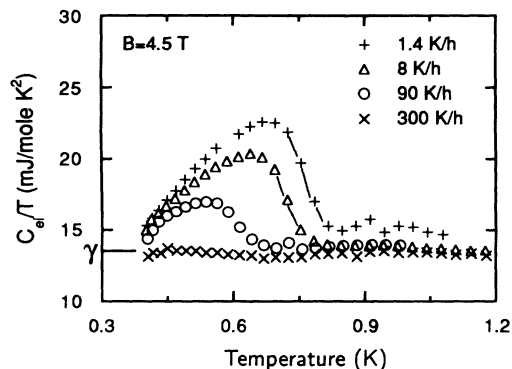


FIG. 1. The electronic specific heat of $(\text{TMTSF})_2\text{ClO}_4$, in molar unit, is displayed in a C_{ei}/T vs T plot, at a fixed field of 4.5 T, for four cooling rates across the anion ordering transition: $dT/dt = 1.4$ (+), 8 (Δ), 90 (\circ), and 300 (\times) K/h. At each cooling rate the specific heat exhibits a jump from the metallic state (horizontal line of amplitude γ), to the semimetallic spin-density-wave state (below the critical temperature). As the cooling rate is increased, the amount of disorder is increased, the critical temperature is lowered, and the height of the specific-heat jump is decreased. Continuous lines are guides for the eye.

5.0 T. The transition between the normal-metal and the FISDW states is characterized by a jumplike anomaly. As it will be discussed later, these jumps are smoothed because of the presence of critical fluctuations. At each magnetic field the result is displayed for several cooling rates: 1.4, 8, 90, and 300 K/h. Two main behaviors are reported: Firstly, the critical temperature decreases as the anion disorder is increased. Secondly, the amplitude of the specific-heat anomaly also decreases.

The electronic specific heat C_{ei} is presented in a C/T

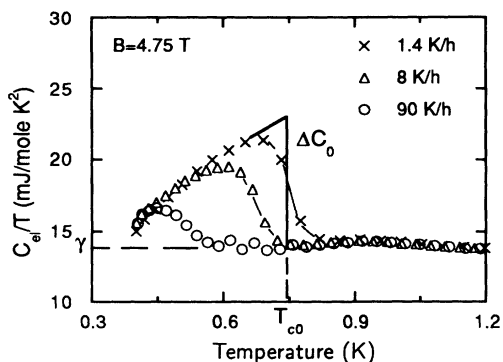


FIG. 2. The evolution of the critical temperature T_c and of the specific-heat jump $\Delta C/T_c$ is displayed at a 4.75-T magnetic field, for three cooling rates: 1.4 (\times), 8 (Δ), and 90 (\circ) K/h. A C/T vs T diagram displays isentropic properties. This means that the unit of area corresponds to the unit of entropy. Since the entropy remains continuous at a second-order transition point, we can build a jump $\Delta C/T_c$ equivalent to the hypothetical mean-field transition, by drawing a vertical segment that gives equal fluctuating areas above and below T_c . The height of the segment multiplied by T_c gives the jump ΔC . The jump ΔC_0 is assigned to the ordered state.

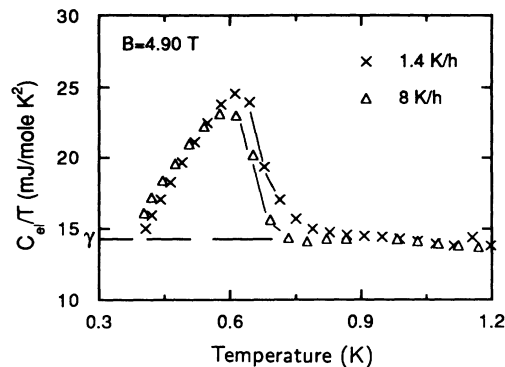


FIG. 3. Evolution of T_c and $\Delta C/T_c$ at a 4.9-T field, for two cooling rates: 1.4 (\times) and 8 (Δ) K/h.

versus T diagram, which is a convenient one for describing electronic phase transitions of second-order, such as the metal-FISDW transition. This is well exemplified in Fig. 2 for the 1.4-K/h cooling rate: (\times) symbols. Above the critical temperature $T_{c0} \approx 0.73$ K, the curve shows first a horizontal line of height γ , characteristic of the metallic state; it exhibits then a jump at the transition; and finally, below T_c , it displays a decrease toward zero as the system enters the semimetallic SDW state. The critical temperature T_c for each cooling rate is determined using the conventional isentropic construction of a second-order phase transition, which takes advantage of the properties of a C/T vs T diagram (the unit area is the unit of entropy, see Fig. 2).

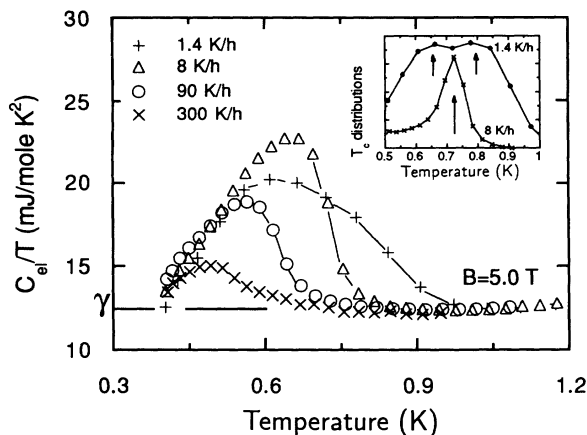


FIG. 4. Evolution of T_c and $\Delta C/T_c$ at a 5.0-T field, for four cooling rates: 1.4 (+), 8 (Δ), 90 (\circ), and 300 (\times) K/h. The insert displays computed distributions of critical temperatures, for 1.4- and 8-K/h curves. The distribution at 8 K/h is sharply peaked at a single T_c , whereas the 1.4-K/h distribution is much broader (almost four times). It can be interpreted as resulting from the close succession of two phase transitions, occurring at $T_{c0} \approx 0.85$ K and $T_{c1} \approx 0.65$ K (upper arrows). The low-temperature anomaly is associated with the tetracritical behavior (see text), which disappears as anion disorder is increased: the specific-heat anomaly becomes single, as displayed by curves (Δ), (\circ), and (\times).

B. A tetracritical behavior

The decrease in the $\Delta C/\gamma T_c$ jump as anion disorder is increased is observed at all fields. However the data presented in Fig. 4 furnish an exception for $B = 5$ T: the 1.4-K/h anomaly (+ symbols) appears to be much broader than the others at faster cooling rates; in fact broader than would yield the mere critical fluctuations or our experimental resolution. In addition, the contrast is strong if we consider the corresponding anomaly at the same rate in Fig. 3, for a very close field ($B = 4.9$ T).

This broadening cannot result from the inhomogeneities inside the sample, or from the gradient of the magnetic field in the volume of the sample, since it only occurs in the most ordered state. It also cannot come from a possible twinning of the single crystal. Moreover, this broadening depends upon the magnetic field.

The broad specific-heat anomaly of Fig. 4 can be tentatively described by a distribution of critical temperatures. The T_c distribution can be evaluated by assuming a simple shape for the specific-heat anomaly. This procedure has been previously used in the case of a superconducting transition.²⁷ The result is shown in the insert of Fig. 4, which displays the distributions obtained for the two cooling rates, 1.4 K/h (dots), and 8 K/h (crosses). The 8-K/h distribution exhibits a sharp peak at $T_c \approx 0.75$ K, with a midheight width $\Delta T_c \approx 0.1$ K. The slower cooling rate of 1.4 K/h leads to a much broader distribution, with a width almost four times larger. It is thus difficult to determine a single mean critical temperature from this kind of distribution. This broad distribution may be interpreted as resulting from two phase transitions with close critical temperatures, T_{c0} and $T_{c1} < T_{c0}$. The shape chosen for the specific-heat anomaly is too crude to give precise quantitative values. Nevertheless, a rough deconvolution leads to $T_{c0} \approx 0.85$ and $T_{c1} \approx 0.65$ K.

In this interpretation, the high-temperature side of the broad anomaly, at T_{c0} , would correspond to the transition from the metal to a first FISDW subphase. The low-temperature transition at T_{c1} would result from a new transition subline arising for a better anion order. As we will see in the following section, this is consistent with the tetracritical behavior we have previously reported.^{18,19} The T_{c1} transition line seems to meet three other lines at a single tetracritical point (following Griffiths' terminology^{28,29}). Thus the effect of anion disorder is to drive the behavior from tetra- to bicritical.¹⁹ An experimental evidence is thus given by Fig. 4: The double anomaly becomes single as the cooling rate is increased from 1.4 to 8 K/h (+ and Δ symbols).

However, the broad specific-heat anomaly does not give as direct an evidence of the tetracritical behavior as the magnetocaloric investigations performed at fixed temperature.^{18,19} This behavior is also characterized by a series of experimental evidences, among which a negative Hall-effect anomaly,¹³ a partial reentrance of the normal metal into the SDW subphases,¹⁸ the existence of a peak in the magnetocaloric effect,¹⁹ and further evidence presented in the following sections.

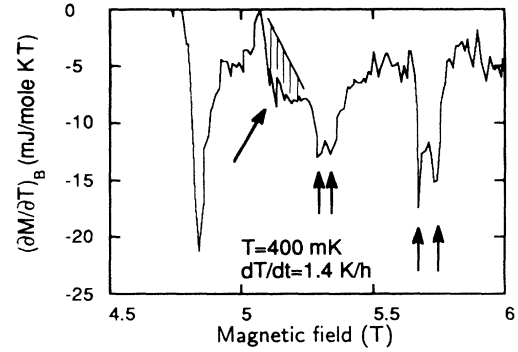


FIG. 5. The isofield coefficient of the magnetization, $\alpha_M = (\partial M/\partial T)_B$, is presented in molar unit as a function of the magnetic field, at a fixed temperature of 400 mK, and for a 1.4-K/h cooling rate. The curve displays a series of large anomalies corresponding to thermodynamic phase transitions between SDW subphases. Notice the anomaly indicated by both the dashed area and the oblique arrow. It is associated with the tetracritical behavior also evidenced in Fig. 4. Double vertical arrows show double anomalies associated with split transition lines.

C. Influence of the cooling rate on the critical fields

The isofield coefficient of the magnetization, $\alpha_M = (\partial M/\partial T)_B$, is plotted versus the magnetic field in Figs. 5 to 8, at two temperatures, $T = 400$ and 500 mK, and for two cooling rates, $dT/dt = 1.4$ and 8 K/h. The following information can be drawn from these data:

(1) α_M displays a series of peaklike anomalies, most of them being indicated by the arrows in Figs. 5 to 8. These anomalies correspond to the phase transformations between adjacent quantized SDW subphases.

(2) The value of α_M is *negative*. This indicates an exothermic transformation at increasing field. Such an α_M vs B plot presents isentropic properties, so that the area of each anomaly corresponds to a negative entropy variation ΔS of the sample, as the field is increased. This means that the electronic system becomes more and more ordered as it enters the higher-field subphases.

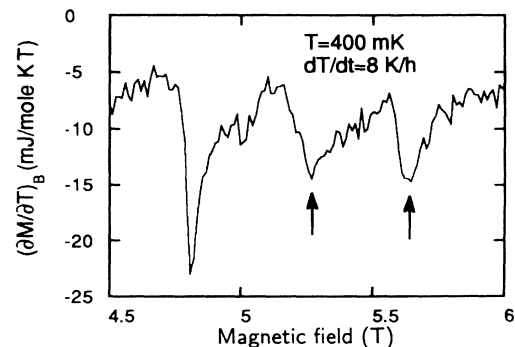


FIG. 6. $(\partial M/\partial T)_B$ vs B plot obtained at the same temperature as Fig. 5, but for a faster cooling rate: $dT/dt = 8$ K/h. Notice the disappearance of the tetracritical anomaly, as well as the vanishing of the splitting process (single arrows).

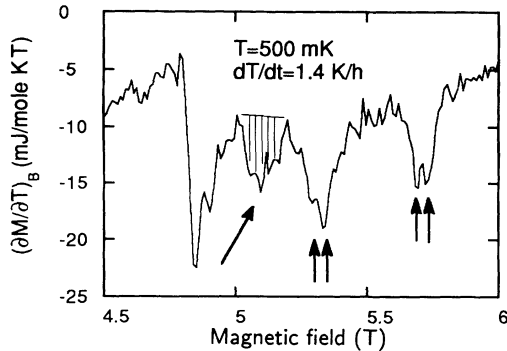


FIG. 7. $(\partial M/\partial T)_B$ vs B plot obtained at the same cooling rate as Fig. 5, but for a higher temperature of 500 mK. The tetracritical anomaly is shifted toward *lower* field (dashed area and oblique arrow).

(3) The tetracritical subline is evidenced by the dashed anomalies in Figs. 5 and 7, and indicated by the oblique arrows.

(4) The critical field $B_c(T)$ of the tetracritical line decreases as the temperature is increased, contrary to the other transition lines (Figs. 5 and 7).

(5) The tetracritical line vanishes as the cooling rate is increased from $dT/dt = 1.4$ to 8 K/h.

(6) Additional anomalies can also be distinguished on these curves. For instance, some peaks exhibit doublets for the slowest cooling rate. They are marked by double vertical arrows in Figs. 5 and 7. They are associated with the fine structure and the arborescent phase diagram previously reported,^{15–17} though the signal-to-noise ratio of the present run is not good enough so as to precise the treelike process. Anyway, the main features are present, and the reproducibility is checked by comparing the data for magnetic fields swept up and down.

(7) Like the tetracritical line, the doublets vanish as the cooling rate is increased from 1.4 to 8 K/h (Figs. 5 and 6).

(8) Moreover, the critical fields B_c , which are determined by the positions of the vanishing α_M doublet

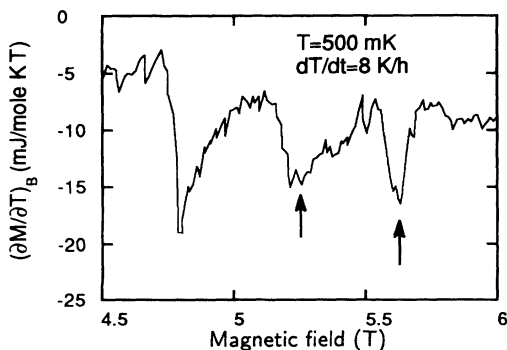


FIG. 8. $(\partial M/\partial T)_B$ vs B plot obtained at $T=500$ mK, for the 8-K/h cooling rate. The tetracritical anomaly has clearly disappeared. See the noticeable shift of the critical fields toward lower field (vertical arrows), as compared with Fig. 7.

anomalies, are shifted toward *lower* fields, as indicated by the vertical arrows in Figs. 5 to 8.

In fact, the shift in the critical field is not monotonic. This can clearly be seen in Fig. 9, which displays the electronic specific heat as a function of the magnetic field in a C_{el}/T vs B plot, at the same temperature as Figs. 5 and 6, $T=400$ mK, and for three cooling rates: $dT/dt = 1.4$, 8, and 90 K/h. The curves were recorded in the same runs as the magnetocaloric measurements. The transitions between the FISDW subphases are characterized by anomalies, either peaklike or smooth cusplike, as indicated by the vertical arrows in Fig. 9. The overall decrease of C_{el} as the field is increased, is a manifestation of the increase in the value of the energy gap opened at the Fermi level by the metal-SDW phase transition.²³ The point is that by increasing the cooling rate from 1.4 to 90 K/h, the critical fields *decrease* as far as the three lower-field transitions are concerned, as displayed by the leftward horizontal arrows in Fig. 9, unlike the highest critical field, which *increases*, as indicated by the rightward horizontal arrow.

D. Arising of a periodicity

These behaviors may appear puzzling and unclear, but it will be shown that it merely results from the arising of a new periodicity in the phase diagram. In effect, a summary of the behaviors can be drawn from the phase diagrams presented in Figs. 10 to 13. The first two diagrams show the disappearance of the tetracritical behavior, in the 4.5–5.5-T field range, whereas the last two display the nonmonotonic variation of the critical fields, between 5.5 to 7 T. Figures 10 and 12 were built from the data obtained for the 1.4- and 8-K/h cooling rates, and Figs. 11 and 13, for the 8- and 90-K/h ones. For each cooling rate, a different symbol is used to describe a point lying

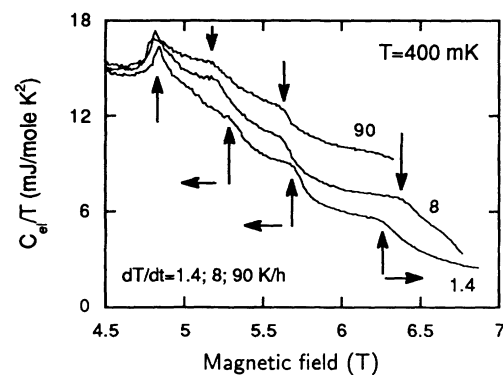


FIG. 9. The electronic specific heat is displayed in a C_{el}/T vs B plot, at a 400-mK temperature, for three cooling rates: $dT/dt = 1.4$, 8, and 90 K/h. Vertical arrows indicate the series of anomalies, which correspond to the phase transitions between SDW subphases. Upward arrows show the critical fields for the most ordered state ($dT/dt = 1.4$ K/h), whereas downward arrows mark the critical fields for the two disordered states. As the cooling rate is increased, notice the shift of the fields toward *lower* fields for the anomalies near the tetracritical transition (leftward horizontal arrows), and the shift toward *higher* fields for the last transition (rightward horizontal arrow).

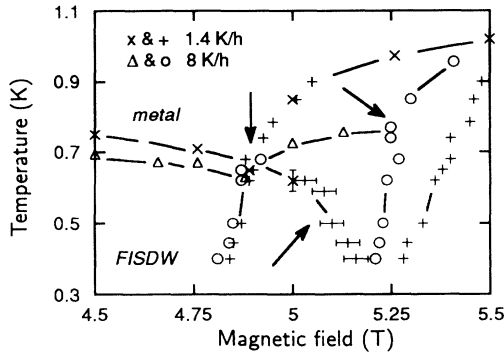


FIG. 10. Evolution of the (B, T) phase diagram of $(\text{TMTSF})_2\text{ClO}_4$ as a function of the cooling rate. For $dT/dt = 1.4$ K/h, (\times) symbols represent $[B, T_c(B)]$ points deduced from C/T vs T experiments (from Figs. 1 to 4), and ($+$) symbols represent $[B_c(T), T]$ points deduced from $(\partial M/\partial T)_B$ vs B or C_{el}/T vs B measurements (among others, from Figs. 5 to 8). Similarly for $dT/dt = 8$ K/h, with (Δ) and (\circ) symbols. The normal-metal phase lies in the high-temperature region. Solid lines are guides for the eye. The vertical arrow marks the position of the tetracritical point. The upward oblique arrow indicates the tetracritical line observed in the most ordered state. This line vanishes as the cooling rate is increased to 8 K/h: the behavior evolves from tetra- to bicritical. The downward oblique arrow shows another bicritical point: see the noticeable shift of its position toward lower field, from 1.4 to 8 K/h.

on a transition line, according to the kind of experiment that was used: In Figs. 10 to 13, (\times) (Δ), and (\diamond) symbols mark the $[B, T_c(B)]$ points deduced from C_{el}/T vs T experiments, for respectively the 1.4-, 8-, and 90-K/h rates, whereas ($+$), (\circ), and (\bullet) symbols represent $[B_c(T), T]$ points deduced from C_{el}/T vs B or α_M vs B experiments, for the same cooling rates.

For the sake of simplicity, the doublet lines are not indicated on the diagrams, nor is shown the arborescent

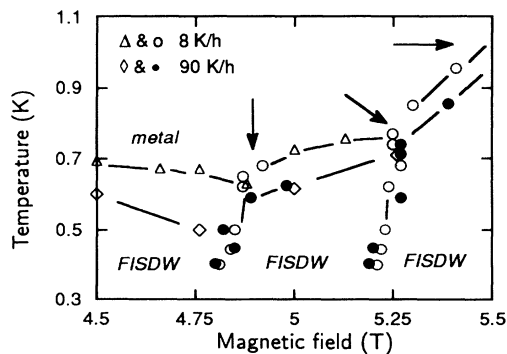


FIG. 11. Phase diagram of $(\text{TMTSF})_2\text{ClO}_4$, with 8-K/h (Δ and \circ symbols) and 90-K/h (\diamond and \bullet symbols) cooling rates. The vertical and oblique arrows indicate the behavior of the bicritical points as the cooling rate is further speeded up. Notice the decrease in the critical temperatures, and the shift of critical fields toward *higher* fields (horizontal arrow). This means that anion disorder destabilizes the FISDW.

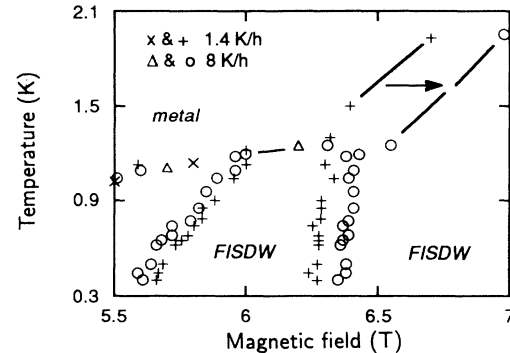


FIG. 12. Phase diagram of $(\text{TMTSF})_2\text{ClO}_4$, showing a higher-field part of the diagram of Fig. 10. Similarly to what is evidenced in Fig. 9, the transition lines move in a nonmonotonic way as the cooling rate is increased: first toward lower fields, and then toward higher fields (rightward arrow). The high-field behavior is analogous to that of Fig. 11: anion disorder destabilizes the FISDW.

character of the tetracritical line, previously reported.^{15–18} This line is indicated by an upward oblique arrow in Fig. 10. It was built using the “dashed” anomalies on magnetocaloric effect curves in Figs. 5 and 7, and using the lower critical temperature deduced from the 1.4-K/h specific-heat curve in Fig. 4. The former critical points are indicated by ($+$) symbols with horizontal error bars, whereas the latter point is marked by a (\times) symbol with a vertical error bar.

The downward vertical arrow in Fig. 10 indicates the location of the tetracritical point. The latter is characterized by the meeting of four transition lines, separating the metallic phase, above the second-order transition line, from two adjacent quantized SDW subphases and a new “intermediate” subphase, below the critical limit.

The phase diagram exhibits several other multicritical points at higher field, but they show no evidence of tetracritical behavior. They appear at the boundaries where adjacent SDW subphases meet the normal phase. They correspond to the merging of two second-order lines into

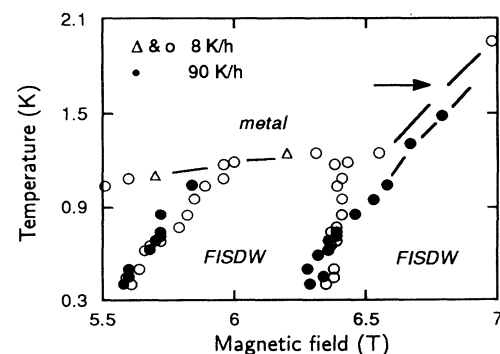


FIG. 13. Phase diagram of $(\text{TMTSF})_2\text{ClO}_4$, showing a higher-field part of the diagram of Fig. 11. The same general behavior as before is observed: the FISDW is destabilized by anion disorder.

one first-order line. They are conventional *bicritical* points: one of them is indicated by the downward oblique arrow in Fig. 10.

As the cooling rate is increased, the behaviors described in the latter sections can be understood within a coherent scheme by examining these phase diagrams. Particularly, the vanishing of the tetracritical behavior is seen to be directly coupled with the nonmonotonic variation of the critical fields. The system behaves as if the anion disorder were locally *favoring* the FISDW at low field, in contradiction with the decrease in the critical temperature, which indicates that the anion disorder *destroys* the FISDW. In fact, the nonmonotonic behavior merely results from the arising of a *periodicity*. This is clearly evidenced in Fig. 10, which shows that the appearance of the tetracritical line (oblique arrow) in between two adjacent transition lines (\circ symbols), makes the latter move away (+ symbols). In other words, the transition lines “relax” toward lower field when the tetracritical line vanishes. This is an indirect experimental evidence for the existence of the tetracritical transition line. Moreover, these results are in good agreement with Hall-effect data, which show a Ribault anomaly in the same field range, that disappears as the cooling rate is increased.¹³

The tetracritical line marks the appearance of a periodicity in the phase diagram. In effect, the SDW subphases of $(\text{TMTSF})_2\text{ClO}_4$ for cooling rates faster than about 2 K/h can be indexed by a series of integer numbers n , determined by the heights of quantized plateaus, and such that n varies roughly linearly as the inverse of the threshold magnetic fields.^{5,13} It appears that no integer number can be attributed to the tetracritical line, which breaks the linear n vs $1/B$ periodicity. Furthermore, the associated Hall anomaly does not form a plateau, and is *negative*.¹³ The tetracritical behavior will be discussed in the following section, using a phenomenological description.

IV. DISCUSSION OF THE ROLE OF ANION ORDERING

A. Comparison with universal pair-breaking

Our experimental data can provide more quantitative information concerning the influence of anion disorder on the metal-FISDW transition, in the neighborhood of the tetracritical point. In Fig. 14, the mean-field jump ΔC is plotted versus the critical temperature T_c ; both are normalized to the “pure” state values ΔC_0 and T_{c0} . The latter are defined at the lowest cooling rate, $dT/dt = 1.4$ K/h. The 5-T anomaly is a special case, due to the presence of the two close phase transitions, so the ΔC_0 jump cannot be measured. We have estimated the value ΔC_0 at $B = 5$ T by assuming the same value $\Delta C/\gamma T_c = 1.4$ as for the $B = 4.9$ T experiment (Fig. 3), with $T_{c0} = 0.85$ K.

A diagram such as Fig. 14 allows us to compare different anion disordered states, without reference to the precise concentration of defects for each cooling rate. The (\times), (\circ), and (\diamond) symbols, respectively, correspond to the fields 4.5, 4.75, and 5.0 T.

Anion ordering produces on the superconducting state

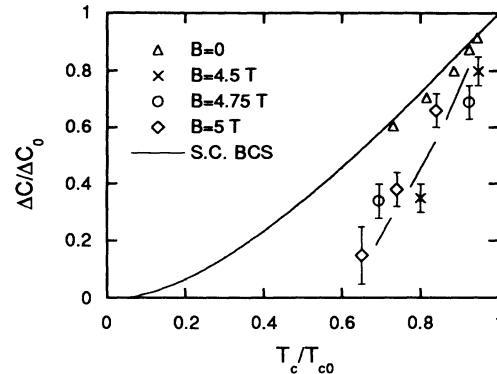


FIG. 14. The variation with anion disorder of the specific-heat jump is displayed in reduced values, in a $\Delta C/\Delta C_0$ vs T_c/T_{c0} plot. Index “0” is assigned to “ordered” state, i.e., to the 1.4-K/h state of our experiments. The correlated decreases in T_c and ΔC can be compared with the universal behavior of a 3D superconductor in presence of magnetic impurities (solid line) (Ref. 31), and with the zero-field behavior of the same compound for similar cooling rates (Δ) (Ref. 30). The results for the FISDW are shown for three magnetic fields: 4.5 (\times), 4.75 (\circ), and 5.0 (\diamond) T (the dashed line is a guide for the eyes). The strong departure from the universal behavior can be interpreted as a strong pair-breaking effect as compared with the superconducting case.

of $(\text{TMTSF})_2\text{ClO}_4$ an effect that is similar to that induced by magnetic impurities in a 3D superconductor. This is indicated on the ΔC vs T_c plot of Fig. 14: previous results on the $B = 0$ superconducting phase are presented by (Δ) symbols,³⁰ together with the universal pair-breaking curve computed for 3D superconductors in presence of magnetic impurities (solid line).³¹

Formally, both superconductivity and a density-wave state may be described as the result of a Bose-Einstein condensation, respectively, of Cooper pairs and of electron-hole pairs.³² Moreover, the same BCS model is expected to apply to both systems.³³ This is indeed observed as far as the specific heat is concerned, at least in the low-field range of the phase diagram.³⁴ By analogy, the effect of anion disorder on the low-field FISDW may be regarded as a pair-breaking effect. From our results two conclusions can be drawn. First, the pair-breaking effect on the FISDW is *qualitatively comparable* with the behavior of the superconducting state. Second, the effect is quantitatively much *stronger* for the FISDW: a strong departure is observed with respect to the universal curve. The jump rapidly reaches a near-zero value at about 60% of T_{c0} (the dashed line in Fig. 14 is a guide for the eyes).

B. Models for the pair-breaking effect

It has long been predicted that the thermodynamic behavior of a CDW or a SDW in presence of nonmagnetic impurities should be analogous to that of the magnetic impurity case of a 3D superconductor.³³ Calculations have been reported by Chang and Maki in the very case of the FISDW in presence of nonmagnetic defects, expecting the same behavior.³⁵ The comparison with our

results on the FISDW shows a qualitative agreement. Nevertheless, this description fails to take into account the quantitative observation.

Moreover, the situation of anion ordering is complicated by the doubling of the lattice periodicity in the transverse direction b , causing the opening of a gap in the energy spectrum. This gap occurs in the region of the reciprocal space where the nesting of the Fermi surface at the SDW wave vector is best achieved. According to the Lebed and Bak model,³⁶ this should not alter the nesting, but make the motion of two particles on two adjacent molecular chains inequivalent. Thus this should weaken the pairing between particles on adjacent chains. The anion ordering gap is then expected to *destroy* the density wave. This means that as the cooling rate increases, the critical temperature of the FISDW should increase. This mechanism could explain the weakening of the zero-field superconducting state in competition with the zero-field SDW, for the benefit of the latter, but the prediction of the model is exactly *contrary* to what we observe in the low-field region of the FISDW: the critical temperature *increases* as the anion gap is better formed (i.e., as the cooling rate is decreased).

Recently, another theoretical model has been proposed in order to take into account the direct effect of the anion-ordering energy gap.^{37,38} Similarly, it describes the modification of the pairing between quasiparticles, due to the potential at the anion-ordering periodicity, which causes the Fermi surface to split into two subbands. This model predicts that the anion gap should only destroy the *even* subphases, keeping the *odd* ones unchanged. This could explain the high-field sequence of Hall plateau values, however at the cost of a disagreement with the lower-field sequence. As the Lebed-Bak model,³⁶ it predicts oscillations of the critical temperatures that are not observed, and it does not take into account our present results: *all* subphases are altered by anion disorder. Moreover, the expected effect is in the *wrong* direction: the critical temperature is observed to *increase* as the value of the invoked anion gap is increased (Figs. 10 to 13).

Incidentally, it can be noted that the situation of $(\text{TMTSF})_2\text{ClO}_4$ is nearly *opposite* to that of $(\text{TMTSF})_2\text{PF}_6$:

(1) The FISDW state in the PF_6 salt has been shown to be closely related to the zero-field SDW state, on either side of the threshold pressure.³⁹ On the contrary, the zero-field SDW and the low-field FISDW in the $(\text{TMTSF})_2\text{ClO}_4$ behave in an opposite way: the former is favored by anion disorder, whereas the latter is destroyed (present results, and Ref. 13).

(2) $(\text{TMTSF})_2\text{PF}_6$ does not exhibit anion ordering, but the effect of irradiation-induced defects has been studied:⁴⁰ the zero-field SDW is destroyed by 0.1% of defects, but the superconducting state, more sensitive, vanishes with only 0.01%. The situation is just reversed as compared with the anion-disorder case of $(\text{TMTSF})_2\text{ClO}_4$, as evidenced in Fig. 14.

These discrepancies can be simply explained if we consider, on the one hand, the nature of disorder: weakly magnetic in the irradiation case,⁴⁰ nonmagnetic in the

anion-disorder case;⁴¹ on the other hand, the nature of the FISDW state: it results from a complex quantization condition.¹¹ The first argument takes into account the strong sensitivity of superconductivity to magnetism, and points out the low-dimensional nature of the superconductivity in $(\text{TMTSF})_2\text{ClO}_4$, which in an unconventional way is destroyed by nonmagnetic disorder. The second argument gives support to the theoretical models of the FISDW: quantum oscillations are well known to be very sensitive to the electronic mean free path, which is reduced by anion disorder.

As a matter of fact, our results cannot exclude a possible role of the anion gap elsewhere in the phase diagram, but it does not seem to play an *active* role in the pair-breaking mechanism.

C. Evolution of the criticality

Several theoretical models have been proposed in order to explain the fine structure^{13–17} of the FISDW phases. Some of them consider the superposition of the order parameters of adjacent quantized subphases, so that new sub-subphases can occur.^{42–44} Such a description allows to qualitatively describe the tetracritical behavior in a very simple scheme, and the tetracritical behavior has been indeed predicted before its experimental observation.⁴² This is a phenomenological description, like Landau's. Consider for instance a system with a two-component order parameter, x and y , coupled biquadratically. The free enthalpy can be developed in powers of x and y :^{29,45}

$$\Delta G = ax^2 + cx^4 + by^2 + dy^4 + 2ex^2y^2. \quad (3)$$

All parameters a to e are assumed to vary as functions of the field B and the temperature T . According to the Landau theory of phase transitions, the conditions $a(B, T) = 0$ and $b(B, T) = 0$ define the continuous transitions between the high-temperature disordered phase (labeled I), and the ordered phases, characterized either by a nonzero x (phase II) or a nonzero y (phase III). As shown in Fig. 15(a), these conditions draw two lines, crossing in

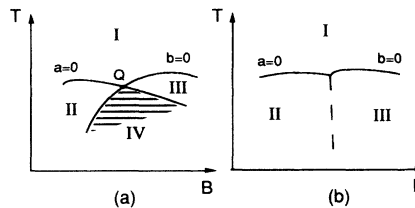


FIG. 15. A tetracritical behavior can be phenomenologically described within the Landau theory of phase transitions. Assume a two-component order parameter, with a biquadratic coupling. Phase labeled I is the symmetric high-temperature phase. In the magnetic field-temperature diagram (a), two continuous transition lines separate the ordered phases II and III from the phase I. These lines cross at a point Q . An “intermediate” phase IV is stable if the coupling is attractive or weakly repulsive (dashed area). If it is too much repulsive, the tetracritical behavior vanishes, so that phases II and III are separated with a discontinuous line, diagram (b).

some point Q , and separating the B - T plane into four quadrants: the three above-mentioned phases, plus a fourth one. The latter, labeled IV, is called the intermediate phase, and corresponds to the superposition of the two order parameters.⁴⁵ In fact, this phase coincides with the fourth quadrant only if the coupling parameter is strictly zero (dashed area in Fig. 15). Particularly, if the coupling is *repulsive*, the size of the existence domain is reduced, and beyond a critical value $e_c = +\sqrt{cd}$, the intermediate phase must vanish. In such a case, the behavior evolves from tetracritical to bicritical. Then the boundary between phases II and III is a first-order line, as indicated in Fig. 15(b).

Within such a description, the phase diagrams presented in Fig. 10 indicate that a hypothetical biquadratic coupling parameter, in the case of $(\text{TMTSF})_2\text{ClO}_4$, would be *positive*, and close to the critical value, since a slight change in the ordering condition is sufficient to drive the behavior from tetracritical to bicritical. Moreover, a repulsive coupling is coherent with the partial reentrance of the metallic phase in the neighborhood of the multicritical point (Figs. 10 and 11), indicating that adjacent subphases weaken each other.

D. Suppression of the fractional phases

Besides the quoted models invoking superposition of FISDW order parameters, a high-order nesting model has been proposed in order to describe the fine structure.⁴⁶ This description takes into account the three key periodicities of the electronic system, say: the SDW wave vector, \mathbf{Q}_{SDW} , the magnetic wave vector, \mathbf{G} , and the longitudinal reciprocal-lattice vector \mathbf{a}^* . Within the framework of the quantized-nesting model, \mathbf{Q}_{SDW} is defined as¹¹

$$\mathbf{Q}_{\text{SDW}} = \left[2k_F + q_{\parallel}, \frac{\pi}{b}, \frac{\pi}{c} \right], \quad (4)$$

where k_F is the Fermi wave vector, b and c being the transverse lattice parameters. This wave vector realizes the nesting of the Fermi surface, causing the metallic phase to disappear to the benefit of the FISDW. The “integer” quantization leads to the following condition for the longitudinal component:¹¹

$$q_{\parallel} = nG = n \frac{eBb}{\hbar}, \quad (5)$$

where e is the electron charge, \hbar is Planck’s constant. n is an integer number; this is the quantum number describing each quantized FISDW subphases.

When the quantization of the wave vector is studied in an extended Brillouin-zone scheme, introducing the lattice period \mathbf{a}^* , rational numbers for the quantization of q_{\parallel} may be found:⁴⁶

$$q_{\parallel} = \frac{s}{m} G, \quad (6)$$

where s is an integer, and m an odd integer. In such a case, the Landau energy bands are split into m subbands. Higher-order nesting conditions may also be found, such as

$$q_{\parallel} = \frac{s}{m + s'/m'} \cdot G \quad (7)$$

and so on, in an iterative way, leading to a further splitting into sub-subbands.⁴⁶ This process leads to a recursive phase diagram that presents similarities with the Azbel-Hofstadter “butterfly.”^{47–49} These rational conditions define the so-called fractional phases. It does not relate to fractionally quantized Hall effect, but this mechanism is able to take into account for the *negative* Hall effect. Unlike the models invoking a superposition of existing order parameters, to each subphase corresponds a new quantum number. As it will be seen, such a mechanism requires high-quality materials, and should be strongly sensitive to disorder.

E. Role of the electronic mean free path

As shown in the beginning of this section, the anion ordering potential does not lead to the expected behaviors, and we suggest that the electronic mean free path plays an unconventional role in these organic materials.

In fact, according to structural studies,⁷ two regimes of disorder can be distinguished as the cooling rate is varied. For $dT/dt < 10$ K/h, Lorentzian profiles for the x-ray-diffusion lines indicate the existence of a random distribution of ordered domains inside the sample, separated by sharp walls. On the other hand, for faster rates, Gaussian profiles would result from clusters of ordered ClO_4 , embedded in a matrix of disordered ClO_4 . The coherence length in the first case never reaches more than 150 nm, whereas in the second case it may decrease down to some tens of nm.⁷ It must be noted that the amount of ordered crystal is close to 100% at an 8-K/h cooling rate, but it is sufficient to destroy the tetracritical behavior, as well as the negative Hall effect,¹³ or the fine structure of the magnetization.¹⁴ Thus, we suggest that the slow dT/dt regime can be separated into two subregimes: below 2 K/h, the crystal is almost fully ordered; the fractional behaviors are observed. Above 2 K/h, the nature of disorder does not change, but the size of domains rapidly decreases as the cooling rate is increased, causing the mean-free path to drop, and the fractional phases to disappear. Because of the mean-free-path reduction, only FISDW phases quantized with *integer* numbers are stable. In the third regime, above 10 K/h, not only the mean free path is reduced, but also disordered domains appear, and a strong pair-breaking effect takes place, destroying the FISDW and restoring a metallic state.

For the slowest cooling rates, the anion gap is not expected to strongly vary, and it is reasonable to assume that the main disorder effect should be a decrease in the electronic mean free path. Moreover, it is worth recalling the large mobility of the $(\text{TMTSF})_2\text{X}$ salts at low temperature:⁵⁰ $\mu \approx 10^5 \text{ cm}^2 \text{ V}^{-1} \text{ s}^{-1} = 10 \text{ T}^{-1}$, which leads to $\omega_c \tau = \mu_B \approx 50$ at $B = 5 \text{ T}$ (ω_c is the cyclotron frequency, and τ is the electron life time). This means that the condition for existence of quantum oscillations is easily fulfilled in the field range of the FISDW.

These compounds are indeed very clean materials. By analogy with the sensitivity of the Ribault anomalies to the amount of anion disorder in $(\text{TMTSF})_2\text{ClO}_4$,¹³ it is

reasonable to assume that the same effect, experimentally reported in $(\text{TMTSF})_2\text{PF}_6$ by several groups,^{39,51,52} can only be observed in the cleanest single crystals. In this respect, the integer behavior of most samples may simply be the signature of imperfect crystals.

Moreover, recent studies on $(\text{TMTSF})_2\text{ClO}_4$ have shown that the anion-ordering transition is suppressed by applying a pressure greater than 5 kbars. As a consequence, the high-field FISDW subphases looks like the ones of $(\text{TMTSF})_2\text{PF}_6$.⁵³ This behavior may be interpreted as the sign that a maximum disorder is favorable to the pure integer quantization, in agreement with the previous statement. However, a possible *active* role of the anion energy gap cannot be ruled out.

Yet, only considering the *passive* role of anion disorder, it is easy to understand why a fractional process, such as that proposed within the high-order-nesting model,⁴⁶ is rapidly destroyed as the mean free path (that is to say, the time τ) is reduced. In effect, the conditions for existence read $\omega_c\tau > 1$ for the integer quantization [Eq. (5)]; $\omega_c\tau > m$ for the fractional condition [Eq. (6)]; $\omega_c\tau > mm'$ for Eq. (7), and so on.^{46,54} The reported mobilities are probably large enough to allow the observation of subphases with m and m' of several units. However the conditions are only fulfilled at low enough temperature, and for samples of high enough quality. Here we are in the presence of an unconventional effect of the electronic mean free path. In fact, as the temperature is decreased, the quantization condition becomes more and more complex, and we should observe a rapidly increasing number of subphases, if the disorder was not limiting the mean free path. The latter would thus play the role of a *cutoff* in the quantization condition. It would not just renormalize electronic interactions, as for a conventional system, but it would govern the very criticality of the phase transitions, which is an unexpected property.

Finally, it can be noted that no theoretical model is able to simultaneously describe the whole physical situation. For example, the predictions of the high-order-nesting model agree with the treelike structure of the phase diagram, and with the observed odd harmonics.^{13,51,17} On the other hand, the superposition models take into account for the tetracritical behavior.⁴²⁻⁴⁴ A nonstandard model has been proposed, also predicting negative Hall plateaus,⁴⁴ but in a chaotic way very different from the observed regularity.^{13,51} Models like that of *Hofstadter* claim that new structures are not expected in the phase diagram if all periodicities are taken into account.⁴⁹

In fact, the exact problem is strongly intricate, and evidently, not exactly soluble. In effect, many characteristic energies of the system have values of the same order of magnitude, i.e., around 10 K: the cyclotron energy, the SDW gap, and anion gap, the interplane coupling, the low-dimensional vibrational modes. . . . No perturbative approach is able to manage such an intermediate-coupling situation. It has been proposed, using ultrametricity arguments, that this situation leads to a series of metastable states described with many order pa-

rameters,⁵⁵ and to a recursive phase diagram similar to the observed one.¹⁵⁻¹⁷ It is plausible that such a phase diagram would be very sensitive to the details of the cooling process, due to the metastabilities resulting from the kinetics effects at the ordering transition.⁵⁵

As we have seen, the direct role of the anion gap is under question. Moreover, attempts of explanations invoking the anion ordering to distinguish the $(\text{TMTSF})_2\text{ClO}_4$ from $(\text{TMTSF})_2\text{PF}_6$ are probably irrelevant. In effect, the deviations from the integer behavior are clearly not the specificity of the first salt, as far as the negative Hall effect is concerned.^{39,51,52} On the contrary, the fractional behavior is perhaps more universal than usually suspected.

V. CONCLUSION

We report the strong pair-breaking effect induced by the anion disorder in the molecular compound $(\text{TMTSF})_2\text{ClO}_4$. Specific-heat investigations in the low-magnetic-field region of the field-induced spin-density-wave phases have shown a strong decrease in the specific-heat jump at the metal-FISDW transition, that is correlated to the decrease in the critical temperature.

Anion disorder also induces strong effects on the criticality of the phase transition lines between SDW subphases: A peculiar point is observed in the phase diagram, which exhibits a tetracritical behavior as the sample is slowly cooled across the anion-ordering transition, transforming into a bicritical behavior as the cooling rate is increased. The arborescent behavior of the transition lines is also suppressed by anion disorder.

More theoretical studies are needed in order to understand the active role of the energy gap produced by the anion ordering in this compound. Nevertheless, a simple scheme invoking the electronic mean free path is sufficient to qualitatively understand the disappearance of the high-order quantization effects, such as the arborescent behavior, or the tetracritical behavior.

Note added. We have recently heard of an independent experimental work, performed in the same region of the phase diagram of $(\text{TMTSF})_2\text{ClO}_4$.⁵⁶ Using similar magnetocaloric investigations, the authors confirm the existence of a tetracritical behavior. With similar data, they interpret differently the thermodynamics of the transitions, proposing a narrower intermediate region. They also confirm the existence of doublet transitions at the slower cooling rates. However, they do not report further arborescence of the transition lines, at least in the temperature region they have investigated (above 0.5 K). They observe a single tetracritical point, in agreement with the present study. They also report new behaviors at higher magnetic fields.⁵⁶

ACKNOWLEDGMENTS

We wish to thank A. G. Lebed', M. Héritier, K. Maki, G. Montambaux, J.-P. Pouget, M. Ribault, and V. M. Yakovenko for fruitful discussions. Laboratoire de Physique des Solides is Unité de Recherche Associée au CNRS.

- ¹P. W. Anderson, *J. Phys. Chem. Solids* **11**, 26 (1959).
- ²J. Bardeen, L. N. Cooper, and J. R. Schrieffer, *Phys. Rev.* **108**, 1175 (1957).
- ³K. Maki, *Superconductivity*, edited by R. D. Parks (Dekker, New York, 1969), Vol. 2, p. 1035.
- ⁴D. Jérôme and H. J. Schulz, *Adv. Phys.* **31**, 299 (1982).
- ⁵For a review of disorder effects on molecular compounds, see, L. Zuppiroli, *Low Dimensional Conductors and Superconductors*, Vol. 155 of *NATO Advanced Study Institute, Series B: Physics*, edited by D. Jérôme and L. G. Caron (Plenum, New York, 1986), p. 307.
- ⁶R. Moret, J.-P. Pouget, S. Ravy, and R. Comès, *Mol. Cryst. Liq. Cryst.* **119**, 257 (1985).
- ⁷J. P. Pouget, S. Kagoshima, T. Tamegai, Y. Nogami, K. Kubo, T. Takijama, and K. Bechgaard, *J. Phys. Soc. Jpn.* **59**, 2036 (1990).
- ⁸P. Garoche, R. Brusetti, and K. Bechgaard, *Phys. Rev. Lett.* **49**, 1346 (1982).
- ⁹T. Takahashi, D. Jérôme, and K. Bechgaard, *J. Phys. (Paris) Lett.* **43**, L565 (1982).
- ¹⁰S. Tomic, D. Jérôme, P. Monod, and K. Bechgaard, *J. Phys. (Paris) Lett.* **43**, L839 (1982).
- ¹¹For both experimental and theoretical reviews on FISDW, see, T. Ishiguro and K. Yamaji, *Organic Superconductors*, Springer Proceedings in Physics, Vol. 88 (Springer, Berlin, 1990); see also review articles by P. M. Chaikin, G. Montambaux, and M. Ribault in *Low Dimensional Conductors and Superconductors* (Ref. 5).
- ¹²For an experimental review of anion ordering, see, J.-P. Pouget, in *Low Dimensional Conductors and Superconductors*, p. 117.
- ¹³M. Ribault, *Mol. Cryst. Liq. Cryst.* **119**, 91 (1985).
- ¹⁴P. M. Chaikin, J. S. Brooks, R. V. Chamberlin, L. Y. Chiang, D. P. Goshorn, D. C. Johnston, M. J. Naughton, and X. Yan, *Physica* **143B**, 383 (1986).
- ¹⁵G. Faini, F. Pesty, and P. Garoche, *J. Phys. Colloq.* **49**, C8-807 (1988).
- ¹⁶F. Pesty, P. Garoche, and M. Héritier, *The Physics and Chemistry of Organic Conductors*, Springer Proceedings in Physics, edited by G. Saito and S. Kagoshima, Vol. 51 (Springer, Berlin, 1990), p. 87.
- ¹⁷F. Pesty and P. Garoche, *Fizika (Zagreb)* **21**, Suppl. 3, 40 (1989).
- ¹⁸F. Tsohnang, F. Pesty, P. Garoche, and M. Héritier, *Synth. Met.* **42**, 1707 (1991).
- ¹⁹F. Tsohnang, F. Pesty, P. Garoche, and M. Héritier, *J. Appl. Phys.* **73**, 5651 (1993).
- ²⁰P. F. Sullivan and G. Seidel, *Phys. Rev.* **173**, 679 (1968).
- ²¹N. W. Ashcroft and N. D. Mermin, *Solid State Physics* (Holt-Saunders, Tokyo, 1981).
- ²²P. Garoche, R. Brusetti, D. Jérôme, and K. Bechgaard, *J. Phys (Paris) Lett.* **43**, L147 (1982).
- ²³F. Pesty, P. Garoche, and K. Bechgaard, *Phys. Rev. Lett.* **55**, 2495 (1985).
- ²⁴N. A. Fortune, J. S. Brooks, M. J. Graf, G. Montambaux, L. Y. Chiang, J. A. A. Perenboom, and D. Althof, *Phys. Rev. Lett.* **64**, 2054 (1990).
- ²⁵P. Weiss and A. Piccard, *C. R. Acad. Sci. Paris* **166**, 352 (1918).
- ²⁶F. Pesty and P. Garoche (unpublished).
- ²⁷P. Garoche, P. Manuel, J. J. Veysié, and P. Molligné, *J. Low Temp. Phys.* **30**, 323 (1978).
- ²⁸R. B. Griffiths, *Phys. Rev. B* **7**, 545 (1973).
- ²⁹L. D. Landau and E. M. Lifshitz, *Statistical Physics, Part I* (Pergamon, Oxford, 1980), p. 497.
- ³⁰F. Pesty, K. Wang, and P. Garoche, *Synth. Met.* **27**, B137 (1988).
- ³¹S. Skalski, O. Betbeder-Matibet, and P. R. Weiss, *Phys. Rev.* **136**, A 1500 (1964).
- ³²W. Kohn and D. Sherrington, *Rev. Mod. Phys.* **42**, 1 (1970).
- ³³P. A. Lee, T. M. Rice, and P. W. Anderson, *Solid State Commun.* **14**, 703 (1974).
- ³⁴F. Pesty, G. Faini, and P. Garoche, *J. Appl. Phys.* **63**, 3061 (1988).
- ³⁵S. R. Chang and K. Maki, *J. Low Temp. Phys.* **66**, 357 (1987).
- ³⁶A. G. Lebed and P. Bak, *Phys. Rev. B* **40**, 11 433 (1989).
- ³⁷T. Osada, S. Kagoshima, and N. Miura, *Phys. Rev. Lett.* **69**, 1117 (1992).
- ³⁸T. Osada, H. Shinagawa, S. Kagoshima, and N. Miura, *Synth. Met.* **56**, 1795 (1993).
- ³⁹J. F. Kwak, J. E. Schirber, P. M. Chaikin, J. M. Williams, H.-H. Wang, and L. Y. Chiang, *Phys. Rev. Lett.* **56**, 972 (1986).
- ⁴⁰M. Y. Choi, P. M. Chaikin, S. Z. Huang, P. Haen, E. M. Engler, and R. L. Greene, *Phys. Rev. B* **25**, 6208 (1982).
- ⁴¹R. Brusetti (unpublished).
- ⁴²A. G. Lebed', *Pis'ma Zh. Eksp. Teor. Fiz.* **51**, 583 (1990) [*JETP Lett.* **51**, 663 (1990)].
- ⁴³K. Machida and M. Nakano, *J. Phys. Soc. Jpn.* **59**, 4223 (1990).
- ⁴⁴V. M. Yakovenko, *Phys. Rev. B* **43**, 11 353 (1991).
- ⁴⁵K.-S. Liu and M. E. Fisher, *J. Low Temp. Phys.* **10**, 655 (1973).
- ⁴⁶M. Héritier, in Ref. 5, p. 243.
- ⁴⁷M. Ya Azbel, *Zh. Eksp. Teor. Fiz.* **46**, 939 (1964) [*Sov. Phys. JETP* **19**, 634 (1964)].
- ⁴⁸D. R. Hofstadter, *Phys. Rev. B* **34**, 2239 (1976).
- ⁴⁹G. Montambaux, *Synth. Met.* **43**, 3807 (1991).
- ⁵⁰J. S. Brooks, M. J. Naughton, R. V. Chamberlin, L. Y. Chiang, and P. M. Chaikin, *J. Magn. Magn. Mater.* **54-57**, 637 (1986).
- ⁵¹B. Piveteau, L. Brossard, F. Creuzet, D. Jérôme, R. C. Lacoé, A. Moradpour, and M. Ribault, *J. Phys. C* **19**, 4483 (1986).
- ⁵²J. R. Cooper, W. Kang, P. Auban, G. Montambaux, and D. Jérôme, *Phys. Rev. Lett.* **63**, 1984 (1989).
- ⁵³W. Kang, S. T. Hannahs, and P. M. Chaikin, *Synth. Met.* **56**, 1936 (1993).
- ⁵⁴M. Héritier, F. Pesty, and P. Garoche, *New Trends in Magnetism*, edited by M. D. Continho-Filho and S. M. Rezende (World Scientific, Singapore, 1990) p. 158.
- ⁵⁵K. Machida, Y. Hori, and M. Nakano, *Phys. Rev. Lett.* **70**, 61 (1993).
- ⁵⁶U. Scheven, W. Kang, and P. M. Chaikan, *J. Phys. IV (Paris) Colloq.* **3**, C2-287 (1993).